⚘ Springer

Correspondence to:
Ikhyun Kim
kimih@kaist.ac.kr

Experimental investigation of the effects of leading edge bluntness on supersonic flow over a double compression ramp

Ikhyun Kim[1,2], Gisu Park[1] and Yung Hwan Byun[3]

[1]Department of Aerospace Engineering, KAIST, Daejeon 305-701, Korea, [2]Department of Engineering Science, The Southwell Building, University of Oxford, Oxford OX2 0ES, United Kingdom, [3]Department of Aerospace Engineering, Konkuk University, Seoul 14370, Korea

Abstract   Understanding the flow characteristics over a double compression ramp is crucial for high-speed vehicle design. Leading edge bluntness is a key factor influencing the formation of a separation region on a double compression ramp flow. In the present study, the effect of bluntness on a double compression ramp is investigated experimentally at a nominal Mach number of 4. The test model has 13º and 40º inclinations with respect to the freestream. Five different levels of leading-edge radius, varying from 0.0 to 2.0 mm, were subjected to supersonic wind tunnel tests. Shadowgraph and infrared thermography techniques were employed to visualize the flow features of the double ramp model. Measurements of surface heat-transfer along the centerline of the test model were obtained from the acquired infrared images. It is shown that the leading-edge radius alters the separation characteristics as well as the surface heat-transfer. Possible reasons for such flow characteristics are discussed.

1. Introduction

The compression ramp, one of the most fundamental geometries, is considered in the design of high-speed vehicles. It is known that the flow field of a compression surface is dominated by shock wave/boundary layer interactions that induce extended separations and cause boundary layer instability, and high thermal pressure loads on the surface [1-3]. During supersonic flights, such interactions are likely to be important factors that affect the vehicle performance. Hence, control mechanisms for this flow feature have been the subject of many investigations.

Some studies have reported mechanisms for controlling the separation size of the compression ramp. Understanding the separation characteristics induced by shock wave/boundary layer interactions is crucial for high-speed vehicle engineering and implementation. Among various techniques for controlling separation, blunting the leading edge has been the most widely considered [4, 5].

In the early works of Holden [6, 7], it was revealed that the separation zone first grows until it reaches the critical radius of the leading edge; the separation zone then decreases with further increase of radius at hypersonic Mach number. Many subsequent works focused on links between separation zone size and leading-edge bluntness. Coet and Chanetz [8] performed pressure and heat-transfer measurements of Mach 10 flow using a single compression ramp model and observed that separation zone size was reduced due to the favorable pressure gradient induced by the presence of bluntness. Neuenhahn and Olivier [9] demonstrated Mach 8 flow over a double compression ramp and observed that leading edge bluntness leads to increasing bow shock curvature in the vicinity of the leading edge, thereby altering the separation length. Subsequent works evaluated the boundary layer thickness, sonic height, entropy layer, and pressure differences; effects of bluntness in hypersonic flows were numerically investigated [4, 5, 10]. Recently, the effects of chemical reactions and leading-edge bluntness on shock wave/boundary layer interactions were investigated by Desai et al. [11] at a Mach number of 6 with an in-house computational fluid dynamics solver. As described above, most find-

ings have been restricted to a single compression ramp at high Mach number. Thus, it is essential to understand flow characteristics of a practical configuration, such as a double compression ramp, at relatively low Mach number. The double compression ramp usually represents realistic geometrical components of high-speed vehicles, such as engine inlets, wing body junctions, and control surfaces [12-15].

The main objective of this work is to understand, via experimental investigation, the effect of bluntness on the flow characteristics over a double compression ramp. The experiments were conducted in a supersonic wind tunnel at a freestream Mach number of 4. The feasibility of visualizing the supersonic flow over the double compression ramp by shadowgraph and infrared (IR) thermography techniques was established in principle in our recent work [16-19]. Typical flow features such as occurrence of separation shock, separation region, and reattachment shock over the investigated geometry are reported in our previous studies (see Fig. 1) [16, 17]. In view of the present research aim, double compression ramp geometries with variable degrees of leading-edge bluntness were employed. Shadowgraph visualization, together with the IR thermograph technique, is currently used to investigate the major flow features in the test model.

2. Experimental apparatus

2.1 Supersonic wind tunnel

The experiments were carried out at Konkuk University's supersonic wind tunnel, called the model aerodynamics facility (MAF), as shown in Fig. 2. The facility was originally designed and built by the Institute of Theoretical and Applied Mechanics (ITAM) of the Russian Academy of Sciences. Information on the design, geometric structure, and experimental calibration of the tunnel can be found in Ref. [20]. The tunnel is a blow-down type facility that can produce Mach flow numbers from 2 to 7. The entire system contains high-pressure vessels, an axisymmetric nozzle, a working section, and a diffuser. The diffuser enables decreasing of the pressure inside the closed test section during runs below 0.01 MPa; system produces supersonic flow at the nozzle without any vacuum chamber [20]. The test

section is of free-jet type with dimensions of 320 mm (length) x 226 mm (height) x 200 mm (width), having three windows that provide optical access from the sides and from above. In this study, a 100 mm diameter Mach 4 axisymmetric nozzle is employed. Dry air is used as the working fluid. Tests were conducted at a plenum total temperature T_0 of 290 K, freestream pressure P_∞ of 14 kPa, and freestream Mach number M_∞ of 4.0; corresponding Reynolds number Re_∞ based on the test model height was approximately 4.7×10^6, as can be seen in Table 1. The MAF run time was about 1 s. Calibration experiments were conducted previously and the reliability of supersonic flow for-

Table 1. Test flow conditions [16-18].

Test conditions	
M_∞ (-)	4
T_0 (K)	295
P_∞ (kPa)	14
T_∞ (K)	70
u_∞ (m/s)	673
Re_∞ (-)	4.7×10^6
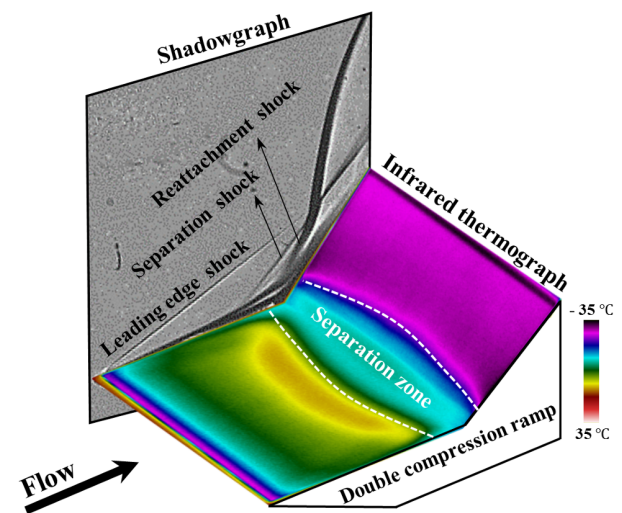
Fig. 1. Schematic of double compression ramp flow [16, 17].

1-air supply; 2-basement; 3-main valve; 4-storage volumes
5-manual valves; 6-time control device; 7-deflector; 8-diffuser
9-test section; 10-contoured nozzle; 11-settling chamber
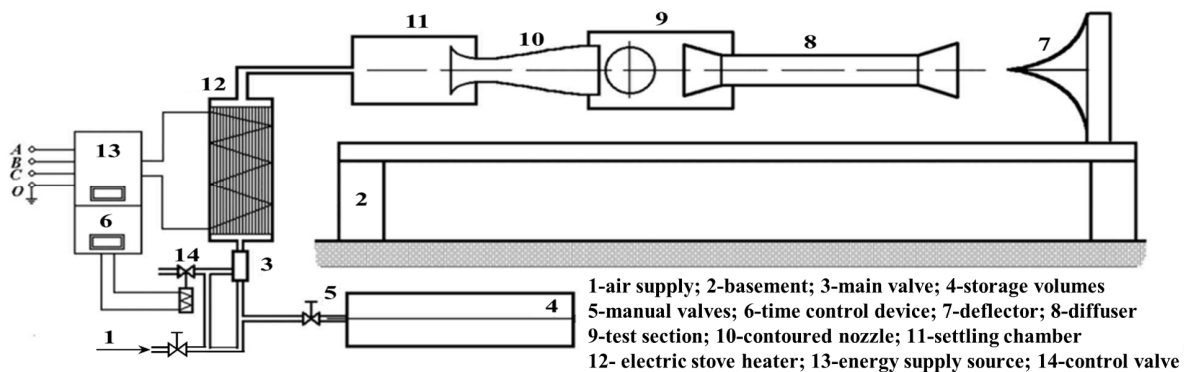12- electric stove heater; 13-energy supply source; 14-control valve

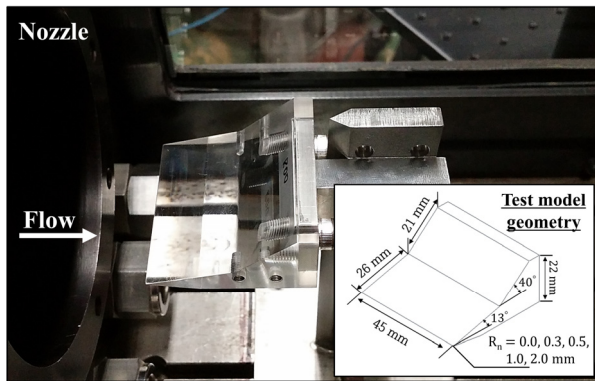Fig. 2. Schematic of supersonic wind tunnel [20].

Fig. 3. Test model in test section.

mation has been demonstrated by various studies, details of which can be found in Refs. [16-23].

2.2 Test model

Fig. 3 shows the test model installed in the test section. The test model is 45 mm wide and 22 mm high. The double compression ramp surfaces have 13º and 40º deflection angles for the first and second ramps, respectively, with respect to the freestream direction. The test model was fabricated from a poly-methyl-methacrylate (PMMA) material, the least conductive material possible, chosen in order to maximize the surface temperature increase for any given test conditions, and satisfying the requirements of the IR thermography technique [17, 24]. Leading edge radius R_n was varied from 0.0 to 2.0 mm.

2.3 Optical diagnostics

Two flow visualization techniques were employed at two different planes. Fig. 4 shows the optical arrangement for the shadowgraph and Infrared (IR) thermography techniques. Full details regarding the optical setup for both visualization techniques are given in our previous works [16-19], so only a brief description is included here. To capture the instantaneous supersonic flow field, a shadowgraph system was implemented consisting of two concave mirrors and standard shadowgraph optics. The red dotted line in the figure represents the light path for the shadowgraph system. An 80 W capacity LED lamp light source was used for the high-speed camera to capture the flow features. A PCO[©] 1600 high-speed camera recorded the images with an exposure time of 100 us. Images were obtained at a sampling rate of 32 kHz and a resolution of 1600 x 1200 pixels.

The transient surface temperature of the test model was recorded by an FLIR[©] A655SC Infrared (IR) thermal imaging camera, which has an operational spectral band of 7.5–14.0 µm. The blue dotted line in the figure denotes the optical path of the IR camera. This camera operates in a standard temperature range of 233 to 423 K, with a reported reading accuracy of ±2 K. The noise equivalent temperature difference for this de-
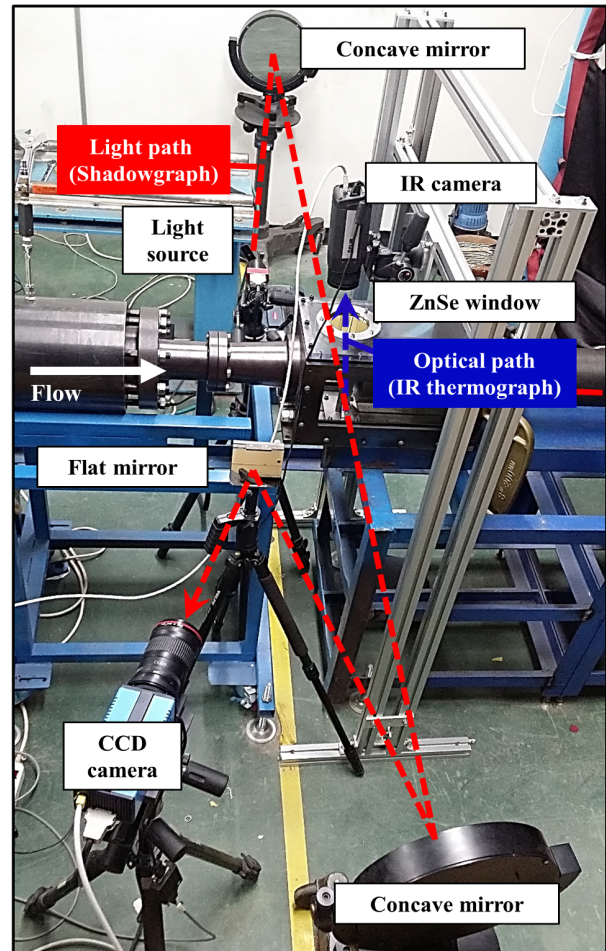

Fig. 4. Photographs of flow visualization setup.

vice is reported at less than 30 mK [25]. Two-dimensional temperature distribution was obtained from IR images taken at a resolution of 640 x 480 pixels and a scanning rate of 50 frames per second. The IR camera was positioned vertically above the test model and fitted with a zinc selenide (ZnSe) window that provides optical access in the corresponding IR wavelength range. At the beginning of the experiments, blackbody-based calibration was performed using an FLIR[©] Commercial Systems Device from the Producers Company, with the help of Eurotherm[©] temperature traceable equipment [18, 19]. This calibration procedure characterized the IR camera detector's response to a series of known blackbody temperatures. The uncertainty associated with the temperature measurement was found to be ±1 K.

At the same time, to guarantee good surface temperature measurements by the IR system, in-situ calibration was performed with a high-accuracy K-type thermocouple taped to the test model. Results agreed with each other with an uncertainty of less than ±0.5 K [18]. The resulting thermal images were processed and analyzed using the FLIR[©] IR V3.3 professional commercial software. The emissivity value of the test model was set at 0.85, known to be the emissivity value of the PMMA

Table 2. Shadowgraph and IR images for different levels of leading-edge bluntness.
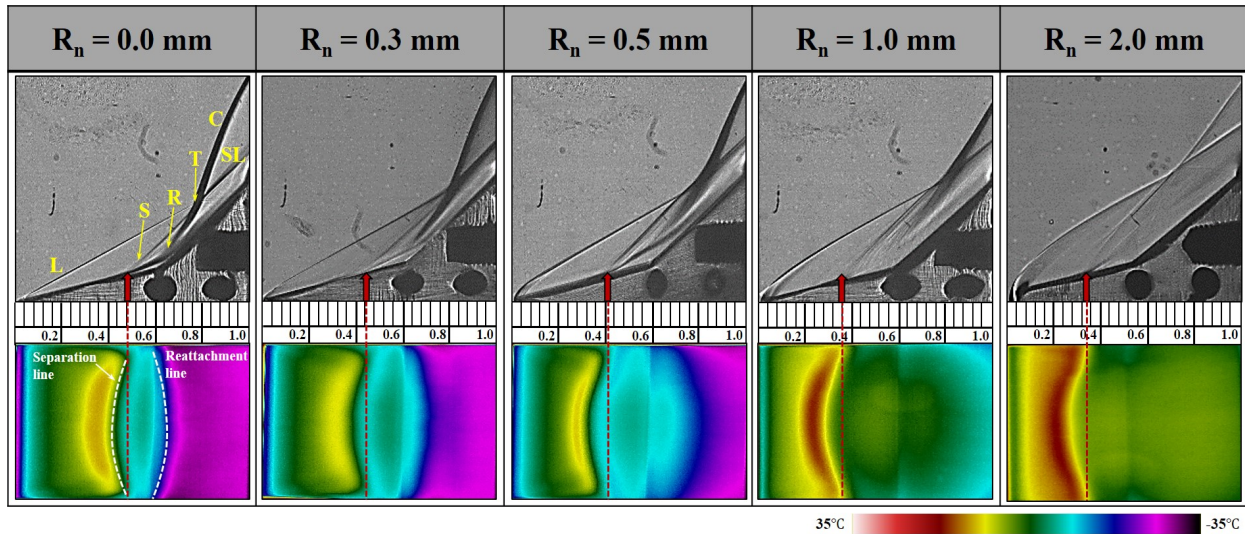
material. The transient temperatures from the thermal images were used to evaluate the heat flux distribution, which is generally applied for the study of flow separation and transition behavior [24-27]. The well-known semi-infinite one-dimensional heat conduction equation proposed by Schultz and Jones [28] was used to determine heat flux q, expressed as,

$$q = \frac{2(\rho c_p \kappa)^{0.5}}{\pi^{0.5}} \sum_{i=1}^{n} \frac{T(t_i) - T(t_{i-1})}{(t_n - t_i)^{0.5} + (t_n - t_{i-1})^{0.5}} \qquad (1)$$

where ρ, c_p, and κ are the density, specific heat capacity, and thermal conductivity of the test model material (ρ = 1180 kg /m^3, c_p = 1470 J/(kg·K), and κ = 0.2 W/(m·K) for the PMMA [12, 15]). This numerical expression describes the surface heat-transfer at time t_i as a function of the wall temperature $T(t_i)$, which is commonly used in short-duration impulse facilities [26-31].

3. Results and discussion

The shadowgraph images in Table 2 show the changes in the flow pattern for the double compression ramp as the bluntness radius is varied from 0.0 to 2.0 mm. Corresponding IR images of the test model surface are included at the bottom of each subfigure. The flow direction is left to right. Because of the relatively cool freestream flow, the IR overall images indicate temperatures below room temperature. The leading-edge shock (L), separation shock (S), and reattachment shock (R) are clearly visualized in the shadowgraph images. Leading edge shock (L) is formed when supersonic flow encounters the first ramp and a boundary layer develops. However, the present visualization data cannot provide sufficient information to distinguish the boundary layer as turbulent or laminar. In general, the boundary layer flow over the ramp surface will experience laminar-transition-turbulent processes. In case of no detached shock wave ahead of the leading edge, the boundary layer flow can be analyzed in terms of Reynolds number, but

due to the presence of the bow shock wave ahead of the ramp, the flow will be vortical and unsteady as well. Thus theoretical approaches to predict the boundary layer flows may be bearing unreasonable results. The present measurement is not enough to give some information on the boundary layer flow.

Separation shock (S) takes place in front of the separation region and the flow reattaches, generating reattachment shock (R). Strong interaction between the shock wave and the boundary layer can be seen near the flow reattachment region. These shock interactions form a triple (T) point between the slip line (SL) and the combined shock (C). At the location of the separation shock, it can be seen in the IR images that the measured temperature is relatively lower; this is due to the effect of shock-induced flow separation and this has been reported by many previous studies, which show similar trend with the present results [13-15]. IR images show that the lowest surface temperature is along the second ramp because the flow in this region has gone through two shock waves, the initial leading-edge shock and then the reattachment shock [13]. Near the end of the first ramp region, because of flow spillage due to the finite span of the test model, the IR images show spanwise features from the central region toward the separation line and toward the side edges. In this experimental arrangement, there will be unintended three-dimensional flow due to the finite test model and test section size; this has often been an issue of interest. Similar observations regarding the spanwise features of the separation region have been reported by researchers using other experimental techniques such as pressure sensitive paint measurement and oil-flow visualization [13-15]. Recently, numerical analysis by Lee et al. [22] showed that the separation region becomes narrow toward the side edges due to the streamlines near the outer side of the edge passage.

As shown in Table 2, although it can be difficult to see, the separation shock front (denoted by the red arrow) moves upstream along the first ramp as the leading-edge radius in-

creases from 0.0 to 1.0 mm. This movement indicates that increased bluntness results in widening of the size of the separation region. Further increases in the bluntness apparently do not affect the separation shock position. This is possibly thought to be due to the relative thickness of the boundary layer and the entropy layer, which is inevitable in highly blunted configurations [4]. As noted by John and Kulkarni [4], the change in entropy layer thickness may alter the flow properties both at the edge and within the boundary layer, which can affect the trend of changes of separation region. Additionally, it can be seen that the location of the triple point shifts downstream as the bluntness increases. A similar observation can be found in the computational analysis by John and Kulkarni [10]. It is noted that the bluntness increases the magnitude of the favorable pressure gradient, which accelerates the flow behind the leading-edge shock and induces velocity distribution on the boundary layer as it approaches the surface. Consequently, the flow environment affects the separation shock location, separation zone size, reattachment shock location, and triple point location with respect to the corresponding position in the sharp leading-edge case.

In regard to the case of $R_n = 2.0$ mm, it can be seen that shadowgraph and IR images show somewhat different flow patterns. With $R_n = 2.0$ mm, although the bluntness increased, the separation region narrowed its size. This may be due to the different leading-edge shocks formed at the leading edge. Fig. 5 provides an optically zoomed shadowgraph image of the leading-edge region for the case of $R_n = 2.0$ mm. It can be seen that detached curve shock formed at the leading edge. It is evident in the computational analysis findings that the strong detached shock alters the flow properties when flow velocity decreases while temperature and pressure increase in the shock layer [8-10]. These changes might affect the flow features downstream, as can be seen in the figure.

Fig. 6 shows the heat flux distributions along the test model centerline, obtained from IR images, averaged over the steady test time period. The heat fluxes are taken to be negative because they are directed from the test model to the flow. For $R_n = 0.0$ to 1.0 mm, the absolute heat transfer is at a minimum on the first ramp, as is commonly observed at the start of the separation zone [14, 32, 33]. This location moves upstream with increases in the leading-edge bluntness. Immediately, downstream of the separation region, due to a boundary layer reattachment, there is a gradual increase in the absolute magnitude of the heat transfer [33]. A decrease in the absolute magnitude of the heat transfer on the second ramp is observed with increase in the leading-edge radius. The case of $R_n = 2.0$ mm, which showed detached bow shock at the leading edge (see Fig. 5), however, apparently has different heat flux distributions. According to John et al. [5] the presence of detached bow shock creates an entropy gradient normal to the flow of the leading edge. Based on their computational analysis, they stated that this entropy gradient induces a strong vorticity outside the boundary layer and provides a stabilizing effect, reducing the intensity of shock wave/boundary layer interactions.
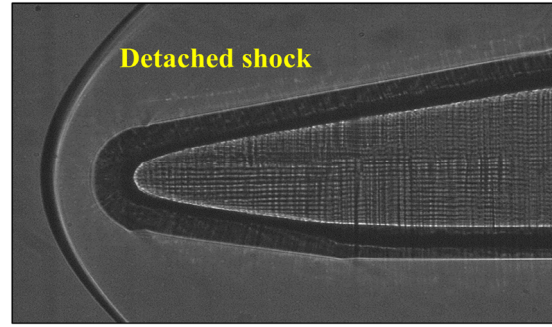

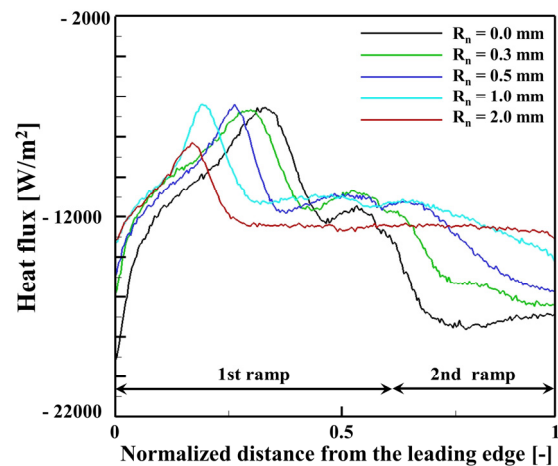Fig. 5. Optically zoomed shadowgraph image for $R_n = 2.0$ mm leading edge.

Fig. 6. Comparison of heat flux distribution along centerline.

As expected from the Crocco's theorem, the strong rotating flow is initiated downstream of the curved shock wave, which will cause the vorticity and entropy production as well, and influence the heat transfer on the ramp surface. In particular, with an increase in the bluntness, the flow unsteadiness due to shock oscillations will be appearing more significant. Unfortunately we cannot make clear such complicated flow features from the present experimental data and will be investigating those flows using three-dimensional CFD study in the subsequent work of the present study.

4. Conclusions

The effect of leading edge bluntness on a double compression ramp has been experimentally investigated in a supersonic wind tunnel. To understand the flow characteristics, the shadowgraph capturing method, along with infrared thermography techniques, was employed. Flow features including separation shock, separation region, and reattachment shock were clearly visualized. It was noticed that even a small level of leading-edge bluntness can alter the flow pattern significantly. Specifically, it has been shown that the start position of the separation zone shifts upstream as the level of leading-edge bluntness increases to 1.0 mm. However, further increases in

bluntness have been found not to significantly affect the corresponding location and led to very few changes in the flow features. From the IR images, spanwise features due to the three-dimensional flow effect in the vicinity of the separation zone were clearly discernible, something which cannot be captured using the standard shadowgraph technique. Flow spillage through the edge side of the finite span was believed to be responsible for these features. Based on the ranges of variables in the present experiments, the increased leading bluntness can be applied to mitigate aerodynamic heating in the vicinity of the second ramp of the realistic high-speed vehicle. The results of the current observations may provide insight into the effects of the bluntness on the flow behavior on a double compression ramp; the authors believe that this study can help in validation and parametric studies for the high-speed vehicle design community.

Acknowledgments

References

[1] J. D. Anderson Jr., *Hypersonic and High Temperature Gas Dynamics*, 2nd Ed., McGraw-Hill, New York, USA (1989) 395-406.

[2] D. Dolling, Fifty years of shock-wave/boundary-layer interaction research: What next?, *AIAA Journal*, 39 (8) (2001) 1517-1531.

[3] D. Gaitonde, Progress in shock wave/boundary layer interactions, *Progress in Aerospace Science*, 72 (2015) 80-99.

[4] B. John and V. Kulkarni, Effect of leading edge bluntness on the interaction of ramp induced shock wave with laminar boundary layer at hypersonic speed, *Computer & Fluids*, 96 (2014) 177-190.

[5] B. John, V. Kulkarni and G. Natarajan, Shock wave boundary layer interactions in hypersonic flow, *International Journal of Heat and Mass Transfer*, 70 (2014) 81-90.

[6] M. S. Holden, Boundary-layer displacement and leading edge bluntness effects on attached and separated laminar boundary layers in a compression corner. Part I : Theoretical study, *AIAA Journal*, 8 (12) (1970) 2179-2188.

[7] M. S. Holden, Boundary-layer displacement and leading edge bluntness effects on attached and separated laminar boundary layers in a compression corner. Part II : Experimental study, *AIAA Journal*, 9 (1) (1971) 84-93.

[8] M. Coet and B. Chanetz, *Experiments on Shock Wave/boundary Layer Interactions in Hypersonic Flow*, English Ed, Rech Aerosp. (1993) 61-74.

[9] T. Neuenhahn and H. Olivier, Influence of the wall temperature and the entropy layer effects on double wedge shock boundary layer interactions, *AIAA Paper 2006-8136* (2006).

[10] B. John and V. Kulkarni, Alterations in critical radii of bluntness of shock wave boundary layer interaction, *Journal of Aerospace Engineering*, 30 (5) (2017) 04017022.

[11] S. Desai, S. Brahmachary, H. Gadgil and V. Kulkarni, Probing real gas and leading-edge bluntness effects on shock wave boundary-layer interaction at hypersonic speeds, *Journal of Aerospace Engineering,* 32 (6) (2019) 04019089.

[12] F. F. J. Schrijer, F. Scarano and B. W. V. Oudheusden, Application of PIV in a Mach 7 double-ramp flow, *Experiments in Fluids*, 41 (2) (2006) 353-363.

[13] L. Yang, H. Zare-Behtash, E. Erderm and K. Kontis, Application of AA-PSP to hypersonic flows: the double ramp model, *Sensors and Actuators B: Chemical*, 161 (1) (2012) 100-107.

[14] L. Yang, H. Zare-Behtash, E. Erdem and K. Kontis, Investigation of the double ramp in hypersonic flow using luminescent measurement systems, *Experimental Thermal and Fluid Science*, 40 (2012) 50-56.

[15] H. Zare-Behtash, K. H. Lo, L. Yang and K. Kontis, Pressure sensitive paint measurements at high Mach number, *Flow Measurement and Instrumentation*, 52 (2016) 10-16.

[16] I. Kim, G. Park, Y. Byun and J. Lee, Experimental study of supersonic flows around a double compression ramp with a sidewall, *Proc. of KSAS Fall Conference* (2015) 55-58.

[17] I. Kim, J. Lee, G. Park, Y. Byun and J. Lee, Test research using an IR thermography technique in a supersonic wind tunnel, *Journal of the Korean Society for Aeronautical & Space Sciences*, 44 (2) (2016) 99-107.

[18] I. Kim, Bluntness effect of double compression ramp in supersonic flow, *Master's Thesis*, Korea Advanced Institute of Science and Technology, Daejeon, Korea (2016).

[19] S. Lee, I. Kim, J. Lee, Y. Byun and G. Park, Distortion correction of surface temperature measurement using an infrared camera, *Journal of the Korean Society for Aeronautical & Space Sciences*, 44 (7) (2016) 545-551.

[20] I. Turko and M. Timofeev, Model aerodynamic facility, *Proc. of KORUS in 7th Korea-Russia International Symposium on Science and Technology*, IEEE Cat. No.03EX737, 1 (2003) 346-350.

[21] W. Choi, D. Seo, J. Lee and Y. Byun, Modification and performance test for improving ability of supersonic/hypersonic wind tunnel (MAF), *Proc. of KSPE Fall Conference* (2010) 717-722.

[22] H. S. Lee, J. H. Lee, G. Park, S. H. Park and Y. H. Byun, Three-dimensional supersonic flow around double compression ramp with finite span, *Shock Waves*, 27 (1) (2017) 69-77.

[23] H. Lee, Y. J. Kim, Y. H. Byun and S. H. Park, Mach 3 boundary layer measurement over a flat plate using the PIV and IR thermography technique, *AIAA Paper 2017-0523* (2017).

[24] F. F. J. Schrijer, Experimental investigation of re-entry aerodynamic phenomena, *Ph.D. Thesis*, Delft University of Technology, The Netherlands (2010).

[25] L. A. Joseph, A. Borgoltz and W. Devenport, Infrared thermography for detection of laminar-turbulent transition in low-speed wind tunnel testing, *Experiments in Fluids*, 57 (5) (2016) 77.

[26] H. Ozawa, S. J. Laurence, J. M. Schramm, A. Wagner and K. Hannemann, Fast-response temperature-sensitive-paint measurements on a hypersonic transition cone, *Experiments in Fluids*, 56 (1) (2015) 1853.

[27] S. J. Laurence, H. Ozawa, J. M. Schramm, C. S. Butler and K. Hannemann, Heat-flux measurements on a hypersonic inlet ramp using fast-response temperature-sensitive paint, *Experiments in Fluids*, 60 (4) (2019) 1-16.

[28] D. L. Shultz and T. V. Jones, *Heat-transfer Measurements in Short-duration Hypersonic Facilities*, AGARDograph-165, North Atlantic Treaty Organization, Advisory Group for Aerospace Research and Development (1973).

[29] I. Kim, S. Lee, G. Park and J. K. Lee, Overview of flow diagnosis in a shock tunnel, *International Journal of Aeronautical and Space Science*, 18 (3) (2017) 425-435.

[30] I. Kim, G. Park and J. J. Na, Experimental study of surface roughness effect on oxygen catalytic recombination, *International Journal of Heat and Mass Transfer*, 138 (2019) 916-922.

[31] I. Kim, S. Lee, G. Park and J. G. Kim, Analysis of nitrogen recombination activity on silicon dioxide with stagnation heat-transfer, *Acta Astronautica*, 177 (2020) 386-397.

[32] H. C. Shi, J. H. Sa, S, H. Park and Y. H. Byun, Transitional flow analysis over double compression ramp with nose bluntness in supersonic flow, *Journal of Computational Fluids Engineering*, 20 (4) (2015) 36-43.

[33] F. Schrijer, Investigation of Görtler vortices in a hypersonic double compression ramp flow by means of infrared thermography, *Quantitative InfraRed Thermography Journal*, 7 (2) (2010) 201-215.

Ikhyun Kim received his Ph.D. degree in 2019 from KAIST. He is currently a Visiting Scholar in the Hypersonic Research Group at Oxford Thermofluids Institute. His research interests include high-speed aerothermodynamics and hypersonic gas-surface interaction.

Gisu Park received his Ph.D. degree in 2010 from the University of New South Wales. He is currently an Associate Professor in the Department of Aerospace Engineering at KAIST. His research interests include hypersonic flows and high-speed ground-tests.

Young Hwan Byun received his Ph.D. degree from the University of Maryland in 1988. He is currently a Professor in the Department of Aerospace Engineering at Konkuk University. His research interests include high-speed ground-tests and shock wave dynamics.